HHS Public Access

Author manuscript

J Magn Reson Imaging. Author manuscript; available in PMC 2020 January 01.

Published in final edited form as:

J Magn Reson Imaging. 2019 January ; 49(1): 291–303. doi:10.1002/jmri.26203.

3D R_2* Mapping of the Placenta During Early Gestation Using Free-Breathing Multiecho Stack-of-Radial MRI at 3 T

Tess Armstrong, MS[1,2], **Dapeng Liu, PhD**[1], **Thomas Martin, MS**[1,2], **Rinat Masamed, MD**[1], **Carla Janzen, MD**[3], **Cass Wong, BS**[1], **Teresa Chanlaw, MPH**[4], **Sherin U. Devaskar, MD**[4], **Kyunghyun Sung, PhD**[1,2], and **Holden H. Wu, PhD**[1,2,*]

[1]Radiological Sciences, University of California Los Angeles, Los Angeles, CA, United States

[2]Physics and Biology in Medicine, University of California Los Angeles, Los Angeles, CA, United States

[3]Obstetrics and Gynecology, David Geffen School of Medicine at UCLA, Los Angeles, CA, United States

[4]Pediatrics, David Geffen School of Medicine at UCLA, Los Angeles, CA, United States

Abstract

BACKGROUND—Multiecho gradient echo Cartesian MRI characterizes placental oxygenation by quantifying R_2*. Previous research was performed at 1.5T using breath-held two-dimensional imaging during later gestational age (GA).

PURPOSE—To evaluate the accuracy and repeatability of a free-breathing (FB) three-dimensional multiecho gradient echo stack-of-radial technique (radial) for placental R_2* mapping at 3T and report placental R_2* during early GA.

STUDY TYPE—Prospective.

POPULATION—30 subjects with normal pregnancies and 3 subjects with ischemic placental disease (IPD) were scanned twice: between 14-18 and 19-23 weeks GA.

FIELD STRENGTH—3T.

SEQUENCE—FB radial.

ASSESSMENT—Linear correlation (concordance coefficient, ρ_c) and Bland-Altman analyses (mean difference, MD) were performed to evaluate radial R_2* mapping accuracy compared to Cartesian in a phantom. Radial R_2* mapping repeatability was characterized using the coefficient of repeatability (CR) between back-to-back scans. The mean and spatial coefficient of variation (CV) of R_2* was determined for all subjects, and separately for anterior and posterior placentas, at each GA range.

*Correspondence to: Holden H. Wu, Ph.D. Department of Radiological Sciences, 300 UCLA Medical Plaza, Suite B119, Los Angeles, CA 90095, Phone: (310) 267-6843, Fax: (310) 825-9118, ORCID iD: 0000-0002-2585-5916, holdenwu@mednet.ucla.edu.

STATISTICAL TESTS—ρ_c was tested for significance. Differences in mean R_2* and CV were tested using Wilcoxon Signed-Rank and Rank-Sum tests. P<0.05 was considered significant. Z-scores for the IPD subjects were determined.

RESULTS—FB radial demonstrated accurate ($\rho_c \geq 0.996$; P<0.001; $|MD| < 0.2 s^{-1}$) and repeatable ($CR < 4 s^{-1}$) R_2* mapping in a phantom, and repeatable ($CR \leq 4.6 s^{-1}$) R_2* mapping in normal subjects. At 3T, placental R_2* mean ± standard deviation was $12.9 s^{-1} \pm 2.7 s^{-1}$ for 14-18 and $13.2 s^{-1} \pm 1.9 s^{-1}$ for 19-23 weeks GA. The CV was significantly greater (P=0.043) at 14-18 (0.63±0.12) than 19-23 (0.58±0.13) weeks GA. At 19-23 weeks, the CV was significantly lower (P<0.001) for anterior (0.49±0.08) than posterior (0.67±0.11) placentas. One IPD subject had a lower mean R_2* than normal subjects at both GA ranges (Z<−2).

DATA CONCLUSION—FB radial provides accurate and repeatable three-dimensional R_2* mapping for the entire placenta at 3T during early GA.

Keywords

R_2* Mapping; Placenta MRI; Free-Breathing MRI; 3D Radial Imaging; 3 T; Early Gestation

INTRODUCTION

Preeclampsia, intrauterine growth restriction (IUGR), and placenta abruption are obstetrical conditions that account for 53% of all medically indicated preterm births less than 35 weeks in the United States (1–4). Collectively, these outcomes are referred to as ischemic placental disease (IPD) and are associated with abnormal placental vascular development, resulting in malperfusion and hypoxia (2–6). Since preterm deliveries due to IPD contribute to higher rates of infant and maternal morbidity and mortality (4), development of accurate methods to predict or detect IPD early in pregnancy would be of great importance to enable prevention strategies and improve outcomes (2).

There are non-invasive methods for assessing placental complications, such as uterine artery (UA) Doppler (2); however, UA Doppler has low sensitivity for the detection of IPD (2, 7), particularly during early gestation and for low risk pregnancies (2, 8). Furthermore, UA Doppler has inter-operator dependencies resulting in inter-operator bias (2).

A promising non-invasive alternative for detecting IPD conditions is magnetic resonance imaging (MRI). MRI can be used to characterize oxygenation in the placenta through quantification of the transverse relaxation rate ($R_2^* = 1/T_2^*$) (9–12). R_2* is known to increase due to local field inhomogeneities caused by deoxyhemoglobin, the form of hemoglobin without oxygen. Thus, R_2* is higher (or T_2* is lower) in hypoxic tissues than in normoxic tissues (9–12). Despite the potential of MRI as a diagnostic tool to detect IPD via R_2* mapping, there is limited understanding of the range of placental R_2* across gestational age (GA), within the structure of the placenta, and among normal and abnormal pregnancies.

Previous investigations of R_2* mapping in the placenta have been performed typically at later GAs from 20-40 weeks using a two-dimensional breath-hold (BH) Cartesian R_2* mapping technique (9–11); with only one very recent study including earlier GAs of 16-40 weeks (12). If IPD is detected at later GA, intervention may not be possible or may have

limited effectiveness (2). In addition, most investigations of R_2* mapping in the placenta were performed using 1.5 T MRI (9–12). Some of these studies showed a significant decrease in nominal placental T_2* as GA increased (9, 10, 12) but in one study, this trend was not significant (11). Compared to 1.5 T, 3 T MRI may provide higher sensitivity to changes in R_2* for detecting IPD. However, to date, there have been limited studies reporting placental R_2* at 3 T (13). Therefore, additional studies are needed to determine the range of placental R_2* for normal and abnormal pregnancies due to IPD at 3 T.

There is evidence of differences in the proportion of abnormal outcomes between anterior and posterior placenta implantation positions. Previous research has shown a higher prevalence of IUGR and placental abruption for anterior placentas compared to posterior placentas (14). For this reason, R_2* characteristics for normal and abnormal pregnancies may differ depending on placenta implantation position. Currently, there is no research reporting the normal or abnormal R_2* separately for anterior versus posterior placentas.

Together with expanding the knowledge of placental R_2*, further work is needed to overcome the technical challenges involved in R_2* mapping in the placenta. In particular, MRI of the placenta can be complicated by both maternal and fetal motion (11, 12, 15, 16) and the irregular position and shape of the placenta among subjects. A major limitation of previous studies is that they use conventional MRI R_2* mapping techniques based on 2D Cartesian sampling, which is sensitive to motion-induced coherent aliasing artifacts. To reduce motion artifacts, scans are acquired during a BH to obtain a single slice (9–12). However, in pregnant patients, involuntary motion can occur during the scan, such as uterine contractions and fetal motion (11, 12, 15, 16). In addition, a BH may not be possible for all patients, such as sick or mentally impaired patients. Even for patients that can perform a BH, requiring a BH may reduce patient comfort during the scan. Due to the limited acquisition time available during a BH (typically 10-20 sec), the spatial coverage, spatial resolution, and image signal to noise ratio (SNR) may be reduced. Finally, placentas can have a range of implantation locations and geometry. Therefore, a free-breathing 3D technique may allow for improved detection of hypoxia throughout the placenta.

Non-Cartesian trajectories, such as 3D stack-of-radial trajectories, have inherent robustness to motion (17–19), potentially allowing for free-breathing (FB) R_2* mapping throughout the entire placenta (13). There have been a few studies performing R_2* mapping using stack-of-radial trajectories in the liver (20–24). Improved image quality using a FB stack-of-radial technique was previously observed for hepatic R_2* mapping compared to conventional BH Cartesian techniques in a population who could not perform a BH (22). One challenge to utilizing non-Cartesian stack-of-radial sampling is its sensitivity to gradient errors (25). To overcome this, a FB 3D stack-of-radial technique with gradient error calibration and correction was recently developed for abdominal imaging (19).

In this study, we propose to evaluate the accuracy and repeatability of a FB radial technique for quantitative R_2* mapping of the placenta in healthy pregnant subjects and abnormal pregnancies due to IPD at early gestation and report R_2* mapping findings at 3 T.

MATERIALS AND METHODS

In Vivo Placenta Study Population

In this IRB-approved study, thirty-three pregnant subjects were recruited and informed consent was obtained. Inclusion criteria were: 18 years of age or older, planning to deliver at a hospital at our institution, carrying a viable pregnancy, not carrying a multifetal gestation pregnancy, absence of known fetal chromosomal or structural abnormalities, no contraindications to MRI, ability to provide consent, and availability for MRI scans during early gestation at two time points: 1. between 14-18 weeks and 2. between 19-24 weeks gestational age (GA). A summary of the study population's clinical characteristics is shown in Table 1. Pregnancies were classified as abnormal due to IPD if a subject displayed at least one of three IPD conditions (preeclampsia, placental abruption, or IUGR) at delivery (i.e., IPD subjects). All other subjects were analyzed as subjects with normal pregnancies (i.e., normal subjects). The normal subjects were also divided into subjects with anterior placental implantation positions (i.e., anterior placenta) and posterior placental implantation positions (i.e., posterior placenta) for separate analysis.

After delivery, thirty subjects were classified as normal subjects while three subjects were classified as abnormal subjects with IPD. One IPD subject was diagnosed with preeclampsia with severe features and two IPD subjects presented with IUGR. Baseline R_2* characteristics were calculated separately for normal subjects (all, anterior placenta, posterior placenta) and IPD subjects. Of the normal subjects, fifteen subjects had anteriorly implanted placentas while fifteen had posteriorly implanted placentas. All of the IPD subjects had anteriorly implanted placentas.

R_2* Mapping using 3D Stack-of-Radial MRI

We used a previously developed multiecho gradient echo sequence based on the golden-angle-ordered 3D stack-of-radial trajectory (FB radial) (19, 26) to obtain images and R_2* maps. Gradient calibration and correction was performed (19). To reduce the scan time to approximately three minutes, all FB radial scans were acquired with two-fold undersampling, as determined by the Nyquist criteria (i.e., number of spokes for fully-sampled data = number of readout points × $\pi/2$). Previous work determined that the R_2* range in the placenta at 3 T was approximately $5 – 25\ s^{-1}$ (13); therefore, twelve echo times with 1.23 ms echo spacing were utilized to improve fitting for this range. For the following phantom and in vivo experiments (See subsections: R_2* Phantom Study and In Vivo Placenta MRI Experiments), all images were acquired on a 3 T MRI scanner (Skyra or Prisma MAGNETOM, Siemens Healthineers, Erlangen, Germany) using a body matrix array and spine array coils.

R_2* Phantom Experiments

A R_2* phantom with ten 50mL test tubes containing an agar gel and ferumoxytol (Feraheme, AMAG Pharmaceuticals Inc., Waltham, MA, United States) was constructed to evaluate R_2* mapping accuracy. The solution was composed of 43 mM (1.2565 g) sodium chloride, 0.043 mM (43.267 μL) gadopentetate dimeglumine (Magnevist, Bayer in Radiology, Warrendale, PA, United States), and 4 g of 3-4% high gel strength agar (Sigma-Aldrich, St. Louis, MO,

United States) dissolved in 500 mL of deionized water. Varying volumes of ferumoxytol were added to each test tube to provide a R_2* range of 5 – 70 s^{-1}, encompassing values previously observed in the placenta at 3 T (13).

The phantom was scanned in the axial orientation using the proposed radial MRI sequence and a commercially-available standard multiecho gradient echo 3D Cartesian MRI sequence (qDixon, the Liver Lab, Siemens, Erlangen, Germany) to evaluate radial R_2* mapping accuracy. A twelve-echo protocol was used for both sequences with imaging parameters matched as much as possible to enable a fair comparison (Table 2). The radial sequence was repeated back-to-back in the same session to assess repeatability (scan 1 and scan 2). A region of interest (ROI) was drawn in each test tube to compare R_2* mapping results between radial and Cartesian sequences.

In Vivo Placenta MRI Experiments

In vivo placenta scans were acquired feet-first supine in each subject with one MRI exam during the time frame of 14-18 weeks GA and then another MRI exam during the time frame of 19-23 weeks GA. Each MRI exam consisted of the axial FB radial sequence (19) and a commercially-available axial T_2 HASTE (27) sequence. Each FB radial scan was acquired with two-fold undersampling and was repeated back-to-back in the same session to evaluate repeatability (scan 1 and scan 2). Representative imaging parameters for FB radial (3D) and T_2 HASTE scans (2D multi-slice) are shown in Table 2.

Reconstruction and R_2* Mapping

Radial MRI reconstruction and signal model fitting were performed offline in MATLAB R2016b (MathWorks, Natwick, MA, USA) using gradient correction (19), 3D gridding, a linear density compensation function, and adaptive coil combination (28). R_2* was calculated using a graph cut algorithm (29–31) by fitting the multiple echo time images to a gradient echo signal model (19, 32, 33) with a seven-peak fat spectrum (34) and a single effective R_2* per voxel (29). Cartesian multiecho images were reconstructed offline in MATLAB and R_2* mapping was performed using the same signal model and fitting algorithm that were used for the radial images. T_2 HASTE images were reconstructed by the scanner software.

In Vivo Placenta Image Analysis

T_2 HASTE and FB radial images were converted to DICOM to be viewed and analyzed in OsiriX 6.0 (Pixmeo Sarl, Bernex, Switzerland). Axial T_2 HASTE images were registered to FB radial images using Advanced Normalization Tools (ANTs) software (35–37). The ANTs registration was performed using 3D non-rigid registration with a mutual information metric used for template matching. Due to low placenta contrast on FB radial images, ROIs were delineated to contour the placenta on registered T_2 HASTE images for all slices. These ROIs were then applied to FB radial images and R_2* maps. An experienced abdominal radiologist (R.M., with 10 years of experience) and an experienced maternal fetal medicine specialist (C.J., with 20 years of experience), both masked to the pregnancy outcome, confirmed the ROI placement on the images and made adjustments if required. The confirmed ROIs were then used to measure the R_2* values over the entire placental volume

for analysis. A diagram illustrating the registration and image analysis steps is shown in Figure 1.

Statistical Analysis

A P-value (P) < 0.05 was considered significant for all statistical analyses. For the phantom experiments, linear correlation and Bland-Altman analysis (38) were performed between radial R_2* and Cartesian R_2*. The equation of the linear regression, Pearson's correlation coefficient (r), Lin's concordance correlation coefficient (ρ_c) (39), mean difference (MD), and limits of agreement (LoA) were calculated for each comparison. r evaluates the strength of the linear relationship between radial R_2* and Cartesian R_2* and ρ_c evaluates the degree of quantitative agreement between radial R_2* and Cartesian R_2* (i.e., if $\rho_c = 1$, radial R_2* = Cartesian R_2*). All correlation coefficients were tested for statistical significance. To assess repeatability for the radial technique, the within-technique mean difference (MD_{within}), the absolute within-technique mean difference (MD_{abs}), within-technique standard deviation (SD_{within}) and coefficient of repeatability (CR) were reported between scan 1 and scan 2 (40, 41).

Only normal subjects were used to determine baseline R_2* characteristics. The mean and range of R_2* were reported. To assess inter-subject temporal variation, slope of the mean R_2* as a function of GA (ΔR_2*), was calculated. To assess intra-subject spatial variation of R_2*, the coefficient of variation (CV), calculated as the standard deviation divided by the mean, was determined for each GA range. With the exception of the range of placental R_2*, all baseline R_2* characteristics were reported as mean ± standard deviation.

Previous research has shown a significantly higher prevalence of IUGR and placental abruption for anterior placentas compared to posterior placentas (14). Therefore, baseline R_2* characteristics were reported for all subjects analyzed together and then separately for two groups (anterior placentas versus posterior placentas). Statistical tests were performed to evaluate differences in mean R_2* between 14-18 weeks GA and 19-23 weeks GA, or between anterior and posterior placentas, using non-parametric Wilcoxon Signed-Rank and Wilcoxon Rank-Sum tests for dependent and independent 2-sample data, respectively. The baseline inter-subject R_2* standard deviation was tested for significant differences using Pittman's test for equality of variances and a 2-sample F-test for dependent and independent data, respectively.

For each individual IPD subject, the mean R_2*, ΔR_2*, and CV were reported. Using these values, the corresponding Z-score (Z) with respect to the normal subjects was calculated as the estimate ($\overline{X}$) minus the population mean (μ) divided by the population standard deviation (σ) (i.e. $Z = \frac{\overline{X} - \mu}{\sigma}$, similar to previous work (9). The corresponding probability ($\hat{P}$) of observing each Z-score was reported.

RESULTS

Accuracy and Repeatability of FB Radial R_2* Mapping

Results from the phantom study found that R_2* measured by Cartesian and radial sequences (scan 1 and scan 2) were consistent (Fig. 2a–b). Linear correlation analysis demonstrated a significant correlation between radial R_2* (scan 1) and Cartesian R_2* ($r = 0.996$, $P < 0.001$; $\rho_c = 0.996$, $P < 0.001$), and between radial R_2* (scan 2) and Cartesian R_2* ($r = 0.998$, $P < 0.001$; $\rho_c = 0.998$, $P < 0.001$) (Fig. 2c). Bland-Altman analysis showed a MD = -0.19 s^{-1} and LoA = [−3.93 s^{-1}, 3.56 s^{-1}] between radial R_2* (scan 1) and Cartesian R_2*, and a MD = 0.04 s^{-1} and LoA = [−2.79 s^{-1}, 2.86 s^{-1}] between radial R_2* (scan 2) and Cartesian R_2* (Fig. 2d). The proposed radial technique demonstrated R_2* mapping repeatability between scan 1 and scan 2 with MD_{within} = 0.23 s^{-1}, MD_{abs} = 0.90 s^{-1}, SD_{within} = 1.41 s^{-1} and CR = 3.90 s^{-1}.

In normal subjects, placental R_2* measured by FB radial scan 1 and scan 2 demonstrated stronger repeatability for 14-18 weeks GA (MD_{within} = 0.32 s^{-1}, MD_{abs} = 0.84 s^{-1}, SD_{within} = 1.05 s^{-1} and CR = 2.92 s^{-1}) than for 19-23 weeks GA (MD_{within} = 0.98 s^{-1}, MD_{abs} = 1.73 s^{-1}, SD_{within} = 2.97 s^{-1} and CR = 8.24 s^{-1}). This was due to two outliers from scans in subjects with posterior placentas during 19-23 weeks GA (See Discussion). A summary of the in vivo placental R_2* mapping repeatability results is shown in Table 3.

In Vivo Placenta Study: Baseline R_2* Characteristics

In vivo placental R_2* maps were successfully obtained from normal subjects (example in Fig. 3) and IPD subjects (example in Fig. 4) with the FB radial technique during early gestation at 3 T. FB radial achieved full volumetric coverage of the placenta in approximately three minutes for all subjects at both time points, except for one normal subject at the second GA time point. This subject had a placenta that extended for more than 176 mm along the superior-inferior direction. Using the same parameters for FB radial as all other subjects (Table 2), 90% of the placenta volume was covered in this subject. Intra-subject spatial heterogeneity of R_2* in the placenta volume was seen on the axial, coronal, and sagittal R_2* maps. For all normal subjects, the inter-subject mean and range of placental R_2* values at 3 T for 14-18 weeks GA was 12.93 s^{-1} ± 2.66 s^{-1} and 7.91 s^{-1} – 20.29 s^{-1}, respectively; and 13.19 s^{-1} ± 1.87 s^{-1} and 9.64 s^{-1} – 16.88 s^{-1} for 19-23 weeks GA (Table 4). The mean R_2* for all subjects at 14-18 weeks and 19-23 weeks GA was not significantly different ($P = 0.530$). The inter-subject standard deviation (SD) of 1.87 s^{-1} was smaller for 19-23 weeks, compared to SD of 2.66 s^{-1} for 14-18 weeks, however this difference was not significant ($P = 0.070$). The mean R_2* for anterior and posterior placentas for 14-18 weeks was 12.93 s^{-1} ± 2.06 s^{-1} and 12.94 s^{-1} ± 3.22 s^{-1} ($P = 0.507$), both of which were similar to the mean R_2* across all subjects. The mean R_2* for anterior and posterior placentas for 19-23 weeks GA was slightly higher for anterior placentas (13.64 s^{-1} ± 1.67 s^{-1}) compared to posterior placentas (12.73 s^{-1} ± 2.01 s^{-1}), but this was not significant ($P = 0.171$). A summary of the baseline mean R_2* and R_2* range results are shown in Table 4.

The FB radial technique was able to utilize full-volume placental R_2* maps to calculate the spatial R_2* variation (CV) and temporal R_2* variation (ΔR_2*). The mean R_2* and CV were

plotted as a function of the GA for all pregnant subjects (Figure 5). For temporal R_2* variation in normal subjects, ΔR_2* was 0.102 ± 0.728, showing a large inter-subject standard deviation. The ΔR_2* for anterior (0.191 ± 0.723) and posterior (0.013 ± 0.747) placentas were not significantly different (P = 0.590). For spatial R_2* variation in normal subjects, the CV was significantly higher for 14-18 weeks GA compared to 19-23 weeks GA with values of 0.632 ± 0.121 and 0.577 ± 0.128, respectively (P = 0.043). For anterior placentas, CV was significantly different between 14-18 weeks GA (0.587 ± 0.108) and 19-23 weeks GA (0.488 ± 0.076) (P = 0.010). For posterior placentas, CV was not significantly different between 14-18 weeks GA and 19-23 weeks GA (P = 0.804). For 14-18 weeks GA, CV was not significantly different between anterior and posterior placentas (P = 0.097). On the other hand, for 19-23 weeks, CV was significantly lower for anterior placentas (0.488 ± 0.076) compared to posterior placentas (0.666 ± 0.106) (P < 0.001). A summary of the baseline ΔR_2* and CV results is shown in Table 4.

In Vivo Placenta Study: IPD Subjects

In three IPD subjects, we measured mean R_2*, ΔR_2*, and CV using FB radial during early gestation at 3 T MRI (Table 5). For the two IPD subjects with IUGR, mean R_2*, ΔR_2*, and CV were similar to baseline values determined in normal subjects. For the IPD subject with preeclampsia, mean R_2* was substantially lower than normal subjects with anterior placentas during 14-18 weeks GA (Z = -2,17, $\hat{P} = 0.030$) and during 19-23 weeks GA (Z = -2.62, $\hat{P} = 0.009$), respectively. Representative axial, coronal reformatted, and sagittal reformatted images of this subject with preeclampsia are shown in Figure 4. Variations in R_2* between the center and the periphery of the placenta along the superior-inferior direction and hot spots with elevated R_2* were observed.

DISCUSSION

In this study, FB 3D stack-of-radial R_2* mapping was performed for the full placental volume in pregnant subjects during early gestation and at 3 T. FB radial demonstrated accurate and repeatable R_2* mapping in a phantom, and repeatable R_2* mapping in subjects with normal pregnancies. Baseline R_2* findings were reported for normal subjects and subjects with IPD at 3 T. In thirty normal subjects, the baseline mean R_2*, ΔR_2*, and CV for 14-18 weeks GA and 19-23 weeks GA were measured and differences in CV were observed between anterior and posterior placentas. Additionally, mean R_2*, ΔR_2*, and CV were successfully obtained in a pilot group of three IPD subjects. Substantial differences in mean R_2* were observed between one IPD subject with preeclampsia and normal subjects. The proposed FB radial technique supports the investigation of placental hypoxia during early gestation by quantifying R_2* throughout the entire placental volume. These 3D R_2* maps can be used to investigate spatial variations in R_2* and temporal changes in R_2* as a function of GA.

With regards to mean R_2* and ΔR_2* at both GA time points, significant differences between anterior and posterior placentas were not observed. Significant differences in the spatial CV of R_2* were observed between 14-18 weeks GA and 19-23 weeks GA, for all subjects and specifically for anterior placentas. For 19-23 weeks GA, significant differences in CV were

observed between anterior and posterior placentas. These observations may be due to biological differences in the vasculature between anterior and posterior placentas. However, another factor to consider is that all subjects were scanned feet-first supine in this study, which might also contribute to these observed differences between anterior and posterior placentas. Further work beyond this study may be required to investigate potential differences between anterior and posterior placentas.

This study investigated earlier GA, while previous studies investigated later GA and a wider GA range (9–12). In some previous studies, a negative correlation between placental T_2* and GA was observed (9, 12) and in one study no significant change in R_2* as a function of GA was observed (11). However, the R_2* behavior at early gestation and 3 T has not been established. Earlier GA may have larger inter-subject R_2* variation compared to later GA due to variations in structural changes in the placenta during early gestation. Therefore, it is not clear that a linear relationship should hold between R_2* and GA during early gestation. Future work includes performing more MRI exams per subject with a larger range of GA to study the behavior of R_2* as a function of GA.

MRI R_2* (or T_2*) mapping may have the potential for detecting IPD. One previous study found significantly higher placental T_2* for normal pregnancies versus IUGR pregnancies (12). Another study showed an improvement in the receiver operating characteristic curve using T_2* mapping for the detection of IUGR, compared to the uterine artery pulsatility index (10). Based on these studies, we expected a higher R_2* to be associated with hypoxia, but in one preeclampsia subject whom we studied, a lower mean placental R_2* compared to normal subjects was observed. Using the FB radial technique to inspect the 3D R_2* maps of the full placental volume, we observed R_2* spatial variation across the placenta with lower R_2* in the center of the placenta and hot spots of higher R_2* along the periphery. Due to the limited knowledge of the behavior of placental R_2* at early gestation in normal and IPD pregnancies, further investigation with additional IPD subjects is needed to determine the relationship between R_2* characteristics and IPD.

Repeatability analysis of FB radial R_2* mapping at 3 T showed better repeatability for all subjects at 14-18 weeks GA (CR ≈ 3 s^{-1}) compared to 19-23 weeks GA (CR ≈ 8 s^{-1}). In the 19-23 weeks GA range, better repeatability was observed for anterior (CR ≈ 5 s^{-1}) compared to posterior placentas (CR ≈ 11 s^{-1}). This was due to two severe outliers, defined as being larger than the 3rd quartile by at least 3 × the interquartile range of the mean differences (42), that were from posterior placentas at 19-23 weeks GA. For these outliers, FB radial scan 1 and scan 2 showed R_2* differences of approximately 7 s^{-1} and 13 s^{-1}. Using the FB radial self-navigation signal (15), we found that these two outliers experienced substantial motion during FB radial scan 2 of 9 mm due to uterine contractions and 23 mm due to bulk patient motion, respectively. These levels of motion were substantially higher than in the other subjects (mean motion = 1.15 ± 1.42 mm, range of motion = 0-8 mm). Since these outliers only occurred during scan 2 and these scans could not be repeated due to scan time constraints, only scan 1 was used to determine mean R_2*, ΔR_2*, and CV. Therefore, these outliers did not affect the baseline R_2* findings, but they did affect the repeatability results. With these outliers removed, repeatability for all subjects and posterior placentas at 19-23 weeks GA was MD_{within} = 0.34 s^{-1}, MD_{abs} = 1.14 s^{-1}, SD_{within} = 1.52 s

$^{-1}$ and CR = 4.20 s^{-1}; and MD_{within} = 0.46 s^{-1}, MD_{abs} = 1.05 s^{-1}, SD_{within} = 1.39 s^{-1} and CR = 3.85 s^{-1}, respectively. To overcome these high levels of motion and improve R_2* mapping, FB radial can be extended to compensate for motion using self-navigation information (15, 43, 44). This will be a topic of future work.

MRI has not been associated with any negative effects on maternal and fetal health, but the benefits vs. risks should be carefully considered before referring pregnant women to MRI. As a general guideline, MRI is typically only performed in medically indicated cases where the benefits outweigh the risks of MRI. The main safety considerations for fetal imaging are the loud noise and biological effects due to time-varying magnetic fields and the specific absorption rate that can cause heating in the subject due to the radiofrequency fields (45). Studies in pregnant women and infants have shown no significant biological effects or adverse events after undergoing MRI (45, 46). To reduce the safety risk due to noise in our study, the total MRI acquisition time was limited to 30 minutes. Furthermore, the FB radial technique used a low flip angle of 5 degrees to limit the specific absorption rate to the subject. For our FB radial technique, the whole body specific absorption rate was 0.08 W/kg and the B_{1+rms} was 0.4 μT.

Our study demonstrates the potential of FB radial 3D R_2* mapping in the placenta, but there are limitations to consider. First, there was reduced placenta contrast on T_1-weighted gradient-echo images compared to T_2-weighted images. Therefore, registration was performed prior to contouring the placenta; however, there may be some errors in the registration. To correct for these errors, ROIs were placed on FB radial images and R_2* maps and then were adjusted by an experienced radiologist and an experienced maternal fetal medicine specialist, masked to the pregnancy outcomes. Second, for the in vivo placenta MRI experiments, a reference BH Cartesian scan was not performed for comparison. Due to scan time and comfort considerations for the pregnant subjects, performing a reference BH Cartesian scan during our study was not practical. Therefore, we performed phantom experiments to evaluate the accuracy of FB radial R_2* mapping with respect to the reference Cartesian method. Third, there are some susceptibility and streaking artifacts on FB radial images and R_2* maps. Susceptibility artifacts can cause increased R_2* in small portions of the placenta if the placenta is oriented near air within the pelvis. To overcome this limitation, ROIs were drawn or adjusted to avoid susceptibility artifacts and this was also confirmed by the experienced radiologist and experienced maternal fetal medicine specialist. Susceptibility artifacts may be mitigated by including quantitative susceptibility mapping and using this to correct for these artifacts (47). FB radial images and R_2* maps may be affected by radial streaking artifacts due to undersampling. In this study, FB radial images were undersampled to reduce the scan time to approximately three minutes. Acquiring fully sampled data or employing non-Cartesian parallel imaging reconstruction techniques, such as ESPIRiT (48), may improve the image quality and mitigate streaking artifacts. Fourth, this was a single-site study with only 30 normal pregnant subjects and 3 IPD subjects. However, our new FB radial technique already demonstrates highly repeatable R_2* mapping at 3 T during early gestation. More subjects will be included in the future to improve our understanding of R_2* characteristics during normal pregnancies. Finally, there were only 3 subjects in our pilot IPD cohort. More IPD subjects will need to

be included in future work to investigate the R_2* characteristics for specific IPD conditions and enable statistical analyses for group comparisons.

In conclusion, we have proposed and evaluated a new FB radial technique for 3D R_2* mapping in the full placental volume in 3 minutes. This technique demonstrated accurate and repeatable R_2* mapping in a R_2* phantom, and repeatable R_2* mapping in normal pregnant subjects. Using FB radial, we measured placental R_2* during early gestation at 3 T. The baseline mean R_2* (±SD) was 12.9 s^{-1} ± 2.7 s^{-1} for 14-18 weeks GA and 13.2 s^{-1} ± 1.9 s^{-1} for 19-23 weeks GA in normal pregnancies. In addition, for all subjects and specifically for anterior placentas, a significantly higher CV was observed for 14-18 weeks GA compared to 19-23 weeks GA. At 19-23 weeks GA, a lower CV was observed for anterior placentas compared to posterior placentas. Compared to normal subjects, one IPD subject had substantially lower mean placental R_2* and different R_2* spatial characteristics at 14-18 weeks and 19-23 weeks GA. FB radial can be used to quantify R_2* in the placenta of pregnant subjects and may be an important tool to further study and improve early detection and management of abnormal pregnancies due to IPD.

Acknowledgments

This work acknowledges the use of the ISMRM Fat-Water Toolbox (http://ismrm.org/workshops/FatWater12/data.htm). The authors would like to thank Irish Del Rosario, Margarida Y. Y. Lei, Dr. Daniel Margolis, Sitaram Vangala, and Aaron Scheffler for their help with this project.

Funding: Research reported in this publication was supported in part by a NIH grant NICHD U01-HD087221.

References

1. Ananth CV, Vintzileos AM. Maternal-fetal conditions necessitating a medical intervention resulting in preterm birth. Am J Obstet Gynecol. 2006; 195:1557–1563. [PubMed: 17014813]
2. Vintzileos AM, Ananth CV. First trimester prediction of ischemic placental disease. Semin Perinatol. 2014; 38:159–166. [PubMed: 24836828]
3. Ananth CV. Ischemic placental disease: A unifying concept for preeclampsia, intrauterine growth restriction, and placental abruption. Semin Perinatol. 2014; 38:131–132. [PubMed: 24836823]
4. Parker SE, Werler MM. Epidemiology of ischemic placental disease: A focus on preterm gestations. Semin Perinatol. 2014:133–138. [PubMed: 24836824]
5. Parks WT. Placental hypoxia: The lesions of maternal malperfusion. Semin Perinatol. 2015; 39:9–19. [PubMed: 25511295]
6. Kingdom JCP, Kaufmann P. Oxygen and placental villous development: Origins of fetal hypoxia. Placenta. 1997:613–621. [PubMed: 9364596]
7. Diagnosis and management of fetal growth restriction. J Pregnancy. 2011; 2011:640715. [PubMed: 21547092]
8. Khong SL, Kane SC, Brennecke SP, Da Silva Costa F. First-trimester uterine artery doppler analysis in the prediction of later pregnancy complications. Dis Markers. 2015; 2015
9. Sinding M, Peters DA, Frøkjær JB, et al. Placental magnetic resonance imaging T2* measurements in normal pregnancies and in those complicated by fetal growth restriction. Ultrasound Obstet Gynecol. 2016; 47:748–754. [PubMed: 26041014]
10. Sinding M, Peters DA, Frøkjær JB, et al. Prediction of low birth weight: Comparison of placental T2* estimated by MRI and uterine artery pulsatility index. Placenta. 2017; 49:48–54. [PubMed: 28012454]
11. Huen I, Morris DM, Wright C, et al. R1 and R2* changes in the human placenta in response to maternal oxygen challenge. Magn Reson Med. 2013; 70:1427–33. [PubMed: 23280967]

12. Sinding M, Peters DA, Poulsen SS, et al. Placental baseline conditions modulate the hyperoxic BOLD-MRI response. Placenta. 2018; 61:17–23. [PubMed: 29277267]
13. Armstrong T, Liu D, Martin T, et al. Free-breathing R2* Characterization of the Placenta During Normal Early Gestation Using a Multiecho 3D Stack-of-Radial Technique. Proc Int Soc Magn Reson Med 25th. 2017:117.
14. Zia S. Placental location and pregnancy outcome. J Turkish Ger Gynecol Assoc. 2013; 14:190–193.
15. Martin T, Liu D, Chanlaw T, et al. Evaluation of placenta motion througout gestation. Proc Int Soc Magn Reson Med 25th. 2017:4802.
16. Sinding M, Peters DA, Frøkjær JB, Christiansen OB, Uldbjerg N, Sørensen A. Reduced placental oxygenation during subclinical uterine contractions as assessed by BOLD MRI. Placenta. 2016; 39:16–20. [PubMed: 26992669]
17. Fujinaga Y, Kitou Y, Ohya A, et al. Advantages of radial volumetric breath-hold examination (VIBE) with k-space weighted image contrast reconstruction (KWIC) over Cartesian VIBE in liver imaging of volunteers simulating inadequate or no breath-holding ability. Eur Radiol. 2016; 26:2790–2797. [PubMed: 26601972]
18. Block KT, Chandarana H, Milla S, et al. Towards routine clinical use of radial stack-of-stars 3D gradient-echo sequences for reducing motion sensitivity. J Korean Soc Magn Reson Med. 2014; 18:87–106.
19. Armstrong T, Dregely I, Stemmer A, et al. Free-breathing liver fat quantification using a multiecho 3D stack-of-radial technique. Magn Reson Med. 2018; 79:370–382. [PubMed: 28419582]
20. Winkelmann S, Schaeffter T, Weiss S, Eggers H, Doessel O. Simultaneous imaging and R2* mapping using a radial multi-gradient-echo (rMGE) sequence. J Magn Reson Imaging. 2006; 24:939–944. [PubMed: 16958064]
21. Lu A, Daniel BL, Pauly JM, Pauly KB. Improved slice selection for R2* mapping during cryoablation with eddy current compensation. J Magn Reson Imaging. 2008; 28:190–198. [PubMed: 18581340]
22. Tipirneni-Sajja A, Krafft AJ, McCarville MB, et al. Radial ultrashort TE imaging removes the need for breath-holding in hepatic iron overload quantification by R2* MRI. Am J Roentgenol. 2017; 209:187–194. [PubMed: 28504544]
23. Krafft AJ, Loeffler RB, Song R, et al. Quantitative ultrashort echo time imaging for assessment of massive iron overload at 1.5 and 3 Tesla. Magn Reson Med. 2017
24. Doyle EK, Toy K, Valdez B, Chia JM, Coates T, Wood JC. Ultra-short echo time images quantify high liver iron. Magn Reson Med. 2017
25. Peters DC, Derbyshire JA, McVeigh ER. Centering the projection reconstruction trajectory: Reducing gradient delay errors. Magn Reson Med. 2003; 50:1–6. [PubMed: 12815671]
26. Winkelmann S, Schaeffter T, Koehler T, Eggers H, Doessel O. An optimal radial profile order based on the golden ratio for time-resolved MRI. IEEE Trans Med Imaging. 2007; 26:68–76. [PubMed: 17243585]
27. Patel MR, Klufas RA, Alberico RA, Edelman RR. Half-fourier acquisition single-shot turbo spin-echo (HASTE) MR: Comparison with fast spin-echo MR in diseases of the brain. Am J Neuroradiol. 1997; 18:1635–1640. [PubMed: 9367310]
28. Walsh DO, Gmitro AF, Marcellin MW. Adaptive reconstruction of phased array MR imagery. Magn Reson Med. 2000; 43:682–690. [PubMed: 10800033]
29. Hernando D, Kellman P, Haldar JP, Liang Z-P. Robust water/fat separation in the presence of large field inhomogeneities using a graph cut algorithm. Magn Reson Med. 2010; 63:79–90. [PubMed: 19859956]
30. ISMRM Fat Water Toolbox. 2012
31. Gleich, DF. Models and algorithms for pagerank sensitivity. Stanford University; 2009.
32. Yu H, Shimakawa A, McKenzie CA, Brodsky E, Brittain JH, Reeder SB. Multiecho water-fat separation and simultaneous R2* estimation with multifrequency fat spectrum modeling. Magn Reson Med. 2008; 60:1122–34. [PubMed: 18956464]
33. Hernando D, Vigen KK, Shimakawa A, Reeder SB. R2* mapping in the presence of macroscopic B0 field variations. Magn Reson Med. 2012; 68:830–840. [PubMed: 22161866]

34. Ren J, Dimitrov I, Sherry AD, Malloy CR. Composition of adipose tissue and marrow fat in humans by 1H NMR at 7 Tesla. J Lipid Res. 2008; 49:2055–2062. [PubMed: 18509197]
35. Advanced Normalization Tools (ANTs).
36. Avants BB, Tustison NJ, Song G, Cook PA, Klein A, Gee JC. A reproducible evaluation of ANTs similarity metric performance in brain image registration. Neuroimage. 2011; 54:2033–2044. [PubMed: 20851191]
37. Avants BB, Yushkevich P, Pluta J, et al. The optimal template effect in hippocampus studies of diseased populations. Neuroimage. 2010; 49:2457–2466. [PubMed: 19818860]
38. Bland JM, Altman DG. Measuring agreement in method comparison studies. Stat Methods Med Res. 1999; 8:135–160. [PubMed: 10501650]
39. Lin LI. A concordance correlation coefficient to evaluate reproducibility. Biometrics. 1989; 45:255–268. [PubMed: 2720055]
40. Bartlett JW, Frost C. Reliability, repeatability and reproducibility: Analysis of measurement errors in continuous variables. Ultrasound Obstet Gynecol. 2008:466–475. [PubMed: 18306169]
41. Obuchowski NA, Reeves AP, Huang EP, et al. Quantitative imaging biomarkers: A review of statistical methods for computer algorithm comparisons. Stat Methods Med Res. 2015; 24:68–106. [PubMed: 24919829]
42. Devore JL. Probability and Statistics for Engineering and the Sciences. 2009
43. Arboleda C, Aguirre-Reyes D, García MP, et al. Total liver fat quantification using three-dimensional respiratory self-navigated MRI sequence. Magn Reson Med. 2016
44. Feng L, Axel L, Chandarana H, Block KT, Sodickson DK, Otazo R. XD-GRASP: Golden-angle radial MRI with reconstruction of extra motion-state dimensions using compressed sensing. Magn Reson Med. 2016; 75:775–788. [PubMed: 25809847]
45. Lisa S, Mary R. Advances and applications in fetal magnetic resonance imaging. Obstet Gynaecol. 2015; 17:189–199.
46. Shao X, Liu D, Martin T, et al. Measuring human placental blood flow with multidelay 3D GRASE pseudocontinuous arterial spin labeling at 3T. J Magn Reson Imaging. 2017
47. Sharma SD, Hernando D, Horng DE, Reeder SB. Quantitative susceptibility mapping in the abdomen as an imaging biomarker of hepatic iron overload. Magn Reson Med. 2015; 74:673–683. [PubMed: 25199788]
48. Uecker M, Lai P, Murphy MJ, et al. ESPIRiT - An eigenvalue approach to autocalibrating parallel MRI: Where SENSE meets GRAPPA. Magn Reson Med. 2014; 71:990–1001. [PubMed: 23649942]

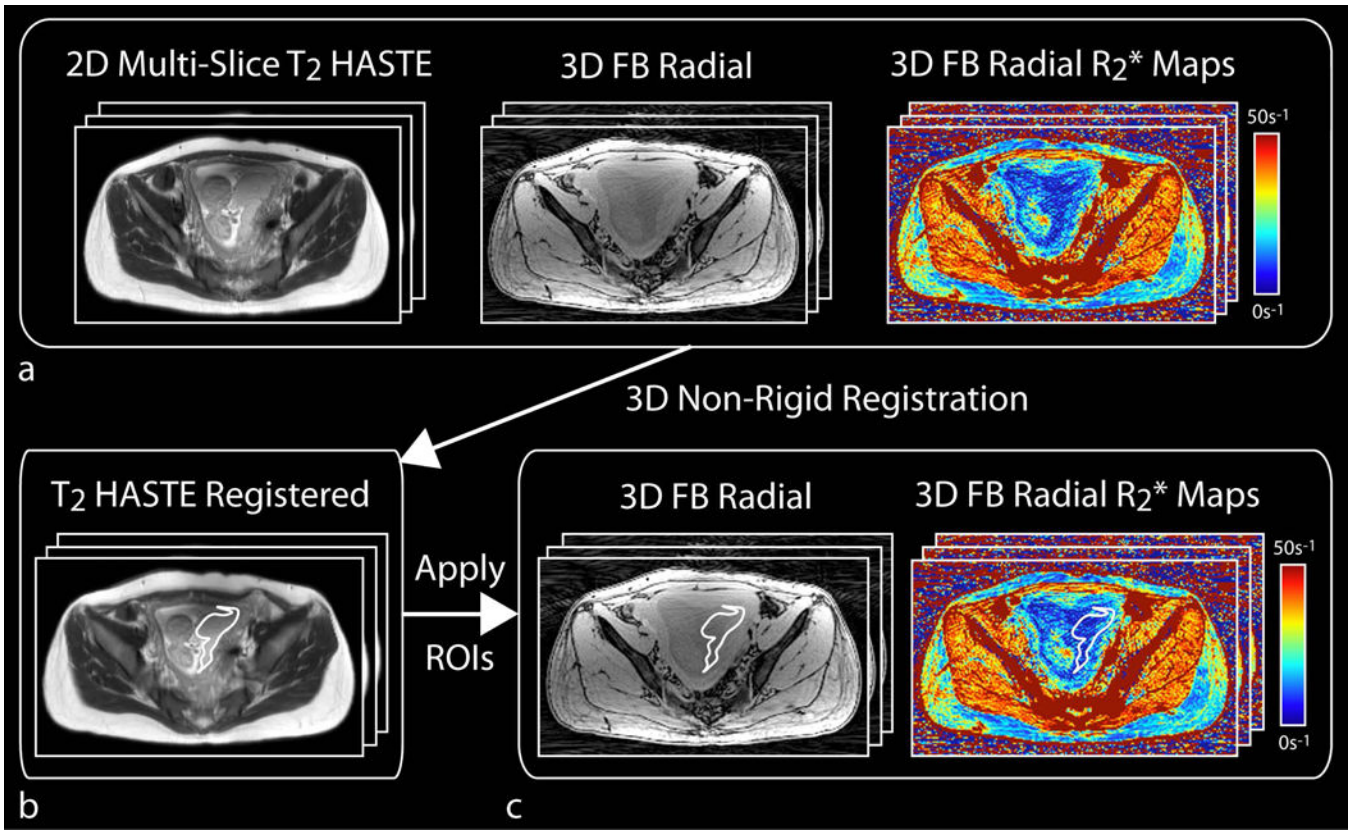

Figure 1.

Diagram of in vivo placenta MRI registration and analysis steps. **(a)** Axial 2D multi-slice T_2 HASTE images were registered using 3D non-rigid registration to the axial 3D free-breathing (FB) radial dataset. **(b)** The registered T_2 HASTE images were used to aid in drawing regions of interest (ROIs) to contour the full placenta volume. **(c)** ROIs were then applied to the 3D FB radial images and R_2* maps, and were confirmed by an experienced radiologist and an experienced maternal fetal medicine specialist. The mean placental R_2* values were measured in the confirmed ROIs.

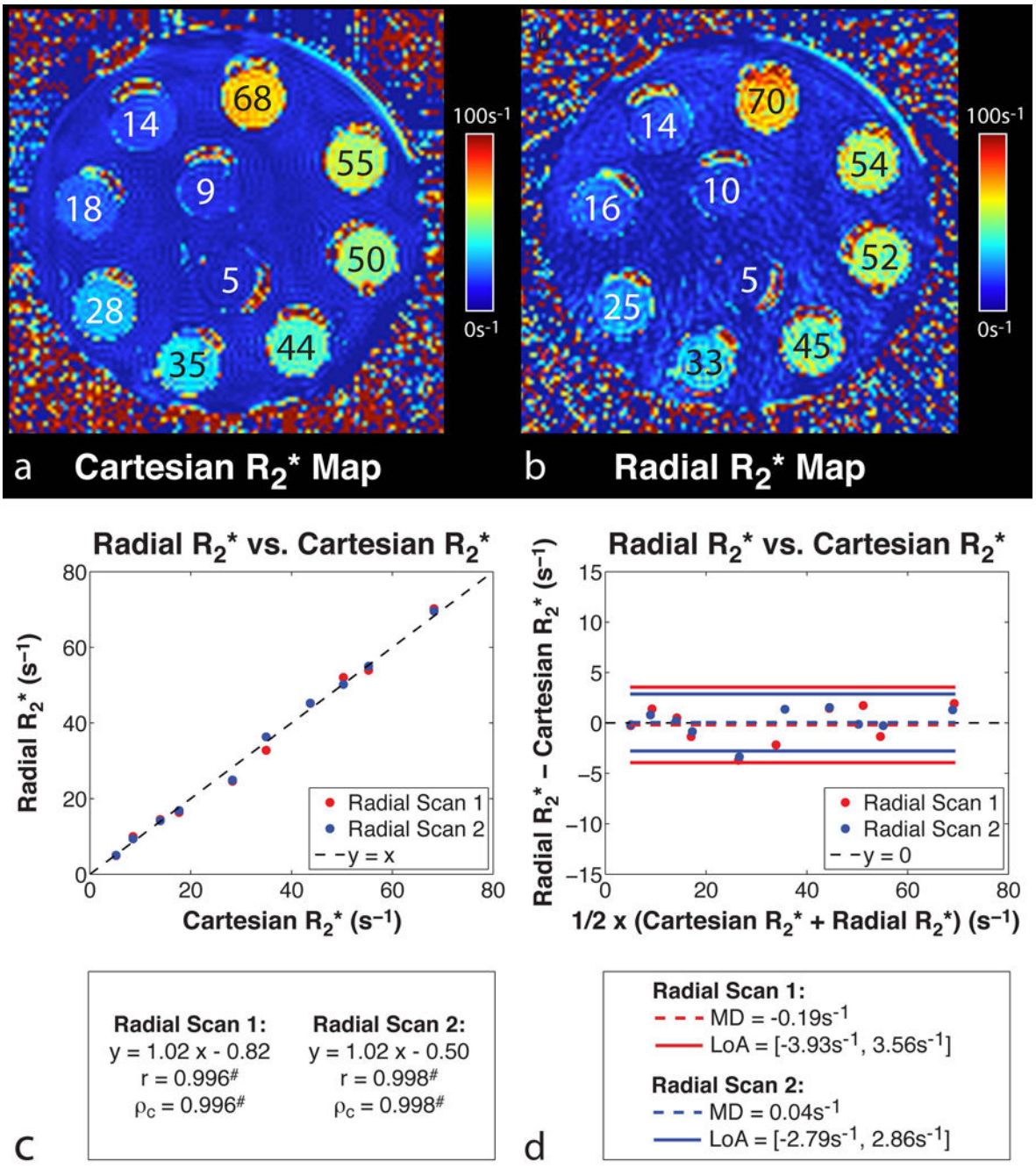

Figure 2.

R_2* maps of the ferumoxytol phantom acquired using the **(a)** Cartesian and **(b)** radial MRI sequences at 3 T in the axial orientation. Test tubes are labeled with their corresponding R_2* values in s^{-1}. R_2* phantom **(c)** linear correlation and **(d)** Bland-Altman analysis results for radial R_2* (scan 1) vs. Cartesian R_2*, and radial R_2* (scan 2) vs. Cartesian R_2* at 3 T. #Statistically significant with $P < 0.001$.

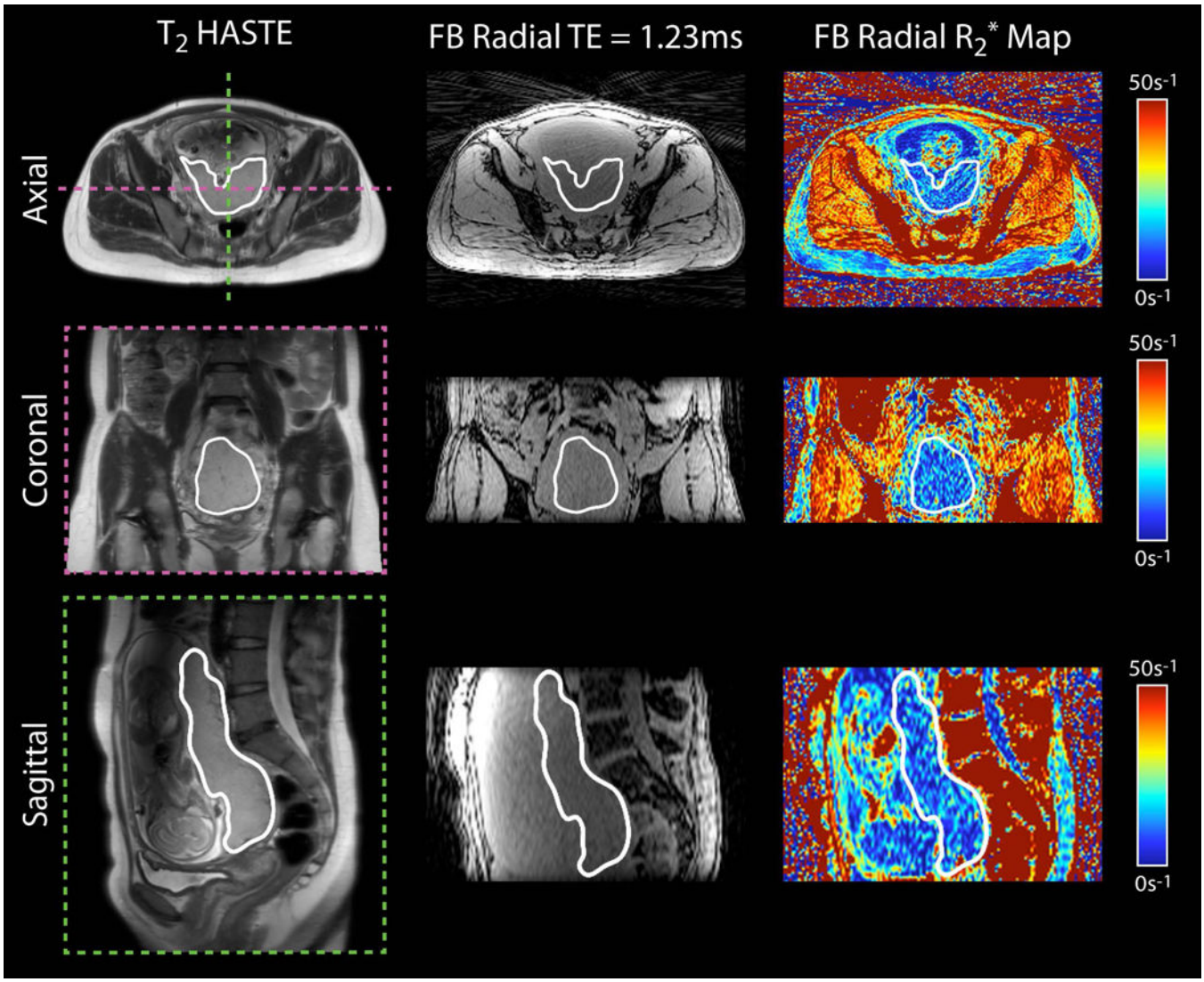

Figure 3.

Representative in vivo placenta images and R_2* maps of a subject with normal pregnancy at 16+2 weeks gestational age acquired using free-breathing (FB) radial MRI at 3 T. Axial, coronal and sagittal views are shown. The placenta is delineated by a white contour.

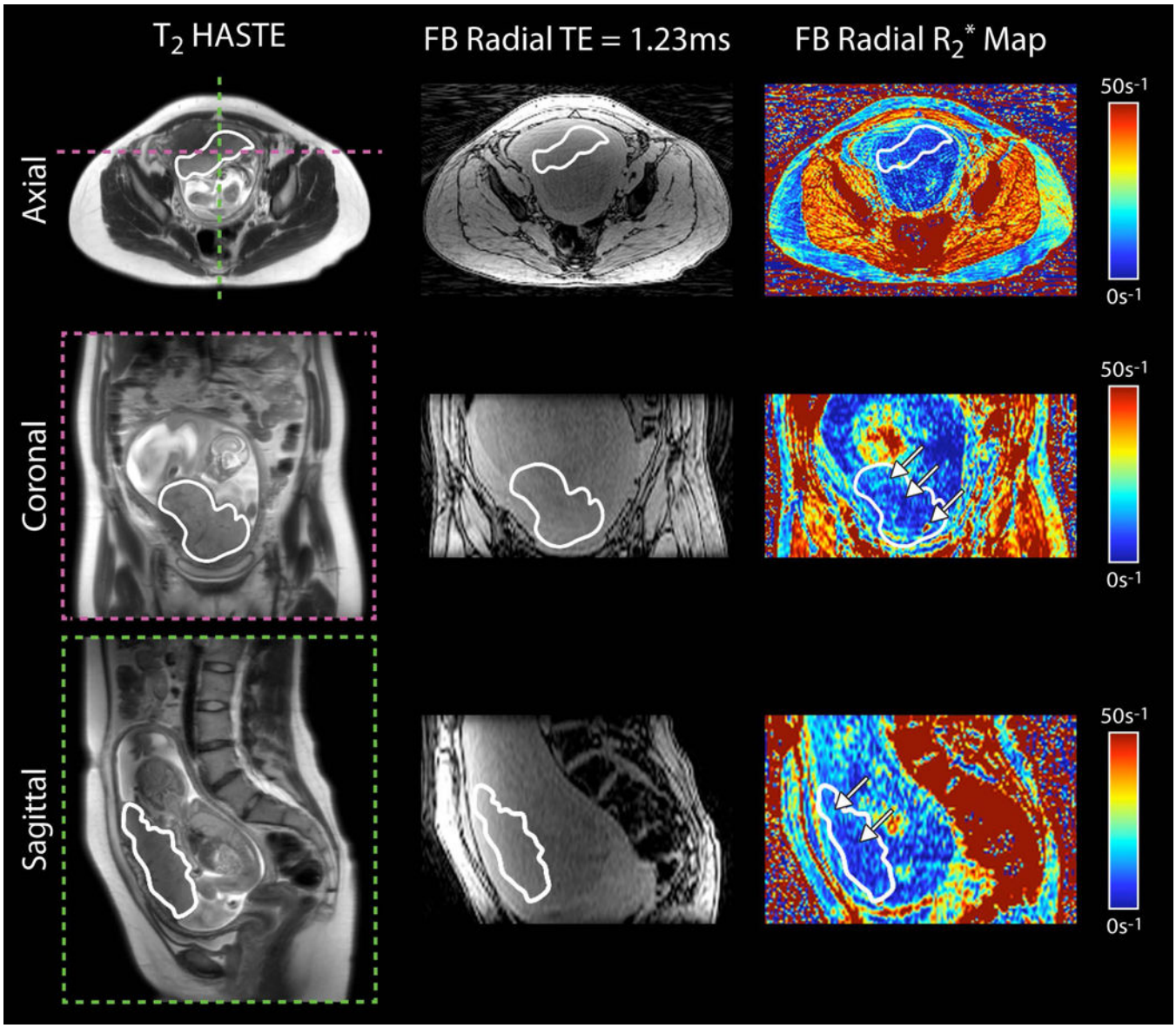

Figure 4.

Representative in vivo placenta images and R_2* maps of a subject with preeclampsia at 19+1 weeks gestational age acquired using free-breathing (FB) radial MRI at 3 T. Axial, coronal and sagittal views are shown. The placenta is delineated by a white contour. White arrows on the R_2* maps point to spatial variation. In this subject, there were regions of higher R_2* along the periphery and regions of lower R_2* in the center of the placenta.

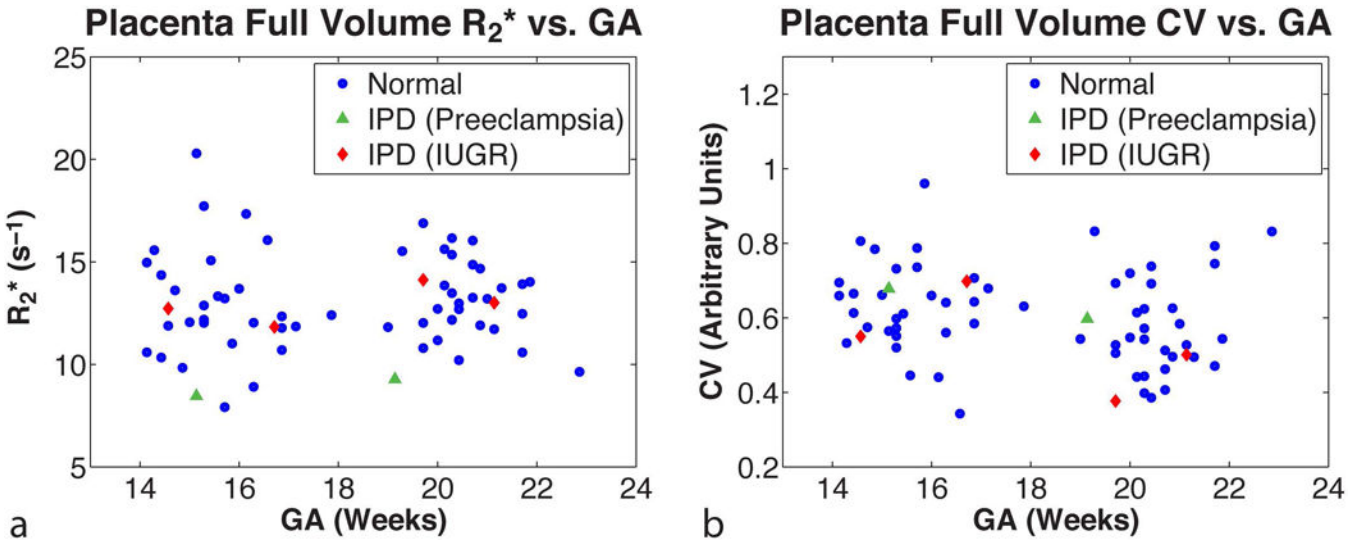

Figure 5.

In vivo placental R_2* measured by free-breathing radial MRI at 3 T. The **(a)** mean placental R_2* (s^{-1}) and **(b)** coefficient of variation (CV) (arbitrary units) are plotted as a function of gestational age (GA) in weeks for the full placental volume. Normal pregnancies (N=30) are shown as blue filled-in circles. Abnormal pregnancies with ischemic placental disease (IPD) (N=3) are shown as green filled-in triangles for preeclampsia and red filled-in diamonds for intrauterine growth restriction (IUGR).

Table 1

Summary of the characteristics for the subjects with normal pregnancies and the subjects with abnormal pregnancies due to ischemic placental disease (IPD).

Maternal Characteristics	Normal Subjects (N = 30)	IPD Subjects (N = 3)
Age at 14-18 Week MRI (Years)	34.31 ± 3.96	33.34 ± 6.05
Body Mass Index (BMI) (kg/m^2)	23.94 ± 4.13	21.73 ± 2.53
BMI Status:		
Underweight	2 (6.7%)	0 (0.0%)
Normal Weight	18 (60.0%)	3 (100.0%)
Overweight	7 (23.3%)	0 (0.0%)
Obese	3 (10.0%)	0 (0.0%)
GA at Delivery (Weeks)	39.43 ± 1.08	39.33 ± 1.44
Delivery Outcome:		
Term	30 (100.0%)	3 (100.0%)
Premature	0 (0.0%)	0 (0.0%)
Delivery Type:		
C-Section	8 (26.7%)	1 (33.3%)
Vaginal Spontaneous	20 (66.7%)	2 (66.7%)
Vaginal Extractor Vacuum	2 (6.7%)	0 (0.0%)
Weight Gain During Pregnancy (lbs)[1]	31.64 ± 12.51	25.57 ± 4.19

Infant Characteristics	Normal Subjects (N = 30)	IPD Subjects (N = 3)
Sex (Male)	17 (56.7%)	2 (66.7%)
Weight (g)	3521.53 ± 384.64	2901.67 ± 502.75
Weight Percentile	50.0% ± 20.8%	16.7% ± 15.9%
Weight Percentile Range	20% − >97%	7% − 35%
Number of Infants With Weight Percentile <10%	0 (0.0%)	2 (66.7%)
Length (cm)[1]	51.89 ± 2.27	46.97 ± 5.21
Length Percentile[1]	62.8% ± 26.7%	31.5% ± 40.3%
Length Percentile Range[1]	7% − >97%	<3% − 60%

Placenta Characteristics	Normal Subjects (N = 27)[2]	IPD Subjects (N = 3)
Weight (g)[3]	465.15 ± 81.26	376.73 ± 46.14
Longest Diameter (cm)	21.65 ± 3.64	20.33 ± 1.53
Umbilical Cord Length (cm)	42.99 ± 13.39	22.17 ± 7.29

[1] One normal subject did not have characteristics due to delivery in another location.

[2]Three normal subjects did not have characteristics due to delivery in another location or elected to keep placenta.

[3]One normal subject had incomplete placental weight due to missing part of placenta.

Table 2

Representative sequence parameters for the phantom and in vivo placenta MRI experiments. The acquisitions were obtained in the axial orientation. A slice oversampling factor of 9.1% was used for all radial acquisitions for the in vivo placenta experiments and a slice oversampling factor of 20% was used for Cartesian and radial acquisitions for the R_2* phantom experiments.

Imaging Parameters	Cartesian (Phantom)	Radial (Phantom)	T_2 HASTE (Placenta)	Radial (Placenta)
Number of Echoes (TE)	12	12	1	12
First TE (ms)	1.23	1.23	92	1.23
ΔTE (ms)	1.23	1.23	N/A	1.23
Last TE (ms)	14.76	14.76	N/A	14.76
Echo Train Length	N/A	N/A	70	N/A
TR (ms)	16.10	16.10	3000	15.90
Matrix(N_x×N_y)	128×128	128×128	272×512	224×224
Field of View (mm_x×mm_y)	220×220	220×220	265×500	380×380
Resolution (mm_x×mm_y)	1.719×1.719	1.719×1.719	0.974×0.976	1.696×1.696
Slice Thickness (mm)	4	4	5	4
Number of Slices	30	30	45	44
Number of Radial Spokes	N/A	126◆	N/A	176◆
Flip Angle (degrees)	5	5	150	5
Bandwidth (Hz/pixel)	1185	1185	390	1175
Scan Time (min:s)	1:14	1:13	2:06	3:16

◆Radial acquisitions were two-fold undersampled based on the Nyquist criteria (i.e. Number of Radial Spokes = $N_X \times \pi/2 \times 1/2$).

Table 3

Repeatability analysis for mean placental R_2* measured in normal subjects using free-breathing radial MRI at 3 T. The within-technique mean difference (MD_{within}), absolute within-technique mean difference (MD_{abs}), within-technique standard deviation (SD_{within}), and coefficient of repeatability (CR) for placental R_2* measured by two back-to-back scans were calculated for all normal subjects (N=30) and again for the subjects separated into anterior (N = 15) versus posterior (N = 15) placenta implantation positions. The analysis was performed for each gestational age (GA) range.

	GA (Weeks)	MD_{within} (s^{-1})	MD_{abs} (s^{-1})	SD_{within} (s^{-1})	CR (s^{-1})
All Subjects (N = 30)	**14-18**	0.32	0.84	1.05	2.92
	19-23	0.98	1.73	2.97	8.24[1]
Anterior (N = 15)	**14-18**	0.48	1.05	1.21	3.37
	19-23	0.24	1.23	1.66	4.60
Posterior (N = 15)	**14-18**	0.15	0.63	0.87	2.42
	19-23	1.73	2.23	3.79	10.50[1]

[1]Includes two severe outliers during the second scan (see Discussion). By removing these outliers, the CR for 19-23 weeks was 4.20 s^{-1} (all subjects) and 3.85 s^{-1} (posterior placenta).

Table 4

Placental R_2* measurements in normal subjects using free-breathing radial MRI at 3 T. Mean R_2* (± standard deviation), R_2* range, coefficient of variation (CV), and mean (± standard deviation) change in R_2* over gestational age (GA) (ΔR_2*) are reported for 14-18 weeks and 19-23 weeks GA. Analysis was performed for all subjects (N = 30), and again for the subjects separated into anterior (N = 15) versus posterior (N = 15) placenta implantation positions.

	GA (Weeks)	R_2* (s^{-1})	R_2* Range (s^{-1})
All Subjects (N = 30)	**14-18**	12.94 ± 2.66	7.91 – 20.29
	19-23	13.19 ± 1.87	9.64 – 16.88
Anterior (N = 15)	**14-18**	12.93 ± 2.06	8.91 – 17.34
	19-23	13.64 ± 1.67	10.80 – 16.88
Posterior (N = 15)	**14-18**	12.94 ± 3.22	7.91 – 20.29
	19-23	12.73 ± 2.01	9.64 – 16.16

	GA (Weeks)	CV (Arbitrary Units)	ΔR_2* (s^{-1}/Week)
All Subjects (N = 30)	**14-18**	0.632 ± 0.121 ◆	0.102 ± 0.728
	19-23	0.577 ± 0.128 ◆	
Anterior (N = 15)	**14-18**	0.587 ± 0.108 ◆	0.191 ± 0.723
	19-23	0.488 ± 0.076 ◆#	
Posterior (N = 15)	**14-18**	0.677 ± 0.120	0.013 ± 0.747
	19-23	0.666 ± 0.106#	

◆ Statistically significant differences with P < 0.05 between 14-18 weeks and 19-23 weeks GA.

Statistically significant differences with P < 0.001 between anterior and posterior placentas.

Table 5

Placental R_2* measurements in subjects with ischemic placental disease (IPD) using free-breathing radial MRI at 3 T. The type of IPD, placenta implantation position (anterior or posterior), mean R_2*, coefficient of variation (CV), and ΔR_2* for 14-18 weeks and 19-23 weeks gestational age (GA) are reported. The Z-score (Z) of each value and the probability ($\hat{P}$) of observing that Z was determined using the population mean from all normal anterior placentas (see Table 4).

Subject	IPD Type, Placenta Implantation Position	GA (Weeks)	R_2* (s^{-1}) Z, $\hat{P}$	CV (Arbitrary Units) Z, $\hat{P}$	ΔR_2* (s^{-1}/Week) Z, $\hat{P}$
1	Preeclampsia, Anterior	14-18	**R_2* = 8.46** ◆ Z = -2.17, $\hat{P}$ = 0.030	**CV = 0.68** Z = 0.84, $\hat{P}$ = 0.399	**ΔR_2* = 0.21** Z = 0.02, $\hat{P}$ = 0.983
		19-23	**R_2* = 9.28** ◆ Z = -2.62, $\hat{P}$ = 0.009	**CV = 0.60** Z = 1.44, $\hat{P}$ = 0.151	
2	IUGR, Anterior	14-18	**R_2* = 12.73** Z = -0.10, $\hat{P}$ = 0.921	**CV = 0.55** Z = −0.34, $\hat{P}$ = 0.734	**ΔR_2* = 0.27** Z = 0.11, $\hat{P}$ = 0.911
		19-23	**R_2* = 14.12** Z = 0.29, $\hat{P}$ = 0.774	**CV = 0.38** Z = -1.46, $\hat{P}$ = 0.143	
3	IUGR, Anterior	14-18	**R_2* = 11.83** Z = -0.54, $\hat{P}$ = 0.591	**CV = 0.70** Z = 1.02, $\hat{P}$ = 0.306	**ΔR_2* = 0.27** Z = 0.11, $\hat{P}$ = 0.916
		19-23	**R_2* = 13.01** Z = −0.38, $\hat{P}$ = 0.703	**CV = 0.50** Z = 0.17, $\hat{P}$ = 0.865	

◆ The probability of observing the Z-score ($\hat{P}$) < 0.05.